





Research Article

Kinetics, Isotherm, Thermodynamics, and Recyclability of Exfoliated Graphene-Decorated MnFe_2O_4 Nanocomposite Towards Congo Red Dye

Van Thinh Pham,^{1,2,3} Hong-Tham T. Nguyen,^{1,2} Thuan Van Tran ^{1,2},
Duyen Thi Cam Nguyen ^{1,2,4}, Hanh T. N. Le,⁵ Thuong Thi Nguyen,^{1,2} Dai-Viet N. Vo,^{1,2}
Thi Hong Nhan Le ⁶ and Duy Chinh Nguyen ⁷

¹NTT Hi-Tech Institute, Nguyen Tat Thanh University, Ho Chi Minh City, Vietnam

²Center of Excellence for Green Energy and Environmental Nanomaterials, Nguyen Tat Thanh University, Ho Chi Minh City, Vietnam

³Graduate University of Science and Technology, Vietnam Academy of Science and Technology, Ha Noi City, Vietnam

⁴Department of Pharmacy, Nguyen Tat Thanh University, Ho Chi Minh City, Vietnam

⁵Institute of Hygiene and Public Health, Ho Chi Minh City, Vietnam

⁶Ho Chi Minh City University of Technology, Vietnam National University-Ho Chi Minh City, Ho Chi Minh City 703500, Vietnam

⁷Center of Excellence for Functional Polymers and NanoEngineering, Nguyen Tat Thanh University, Ho Chi Minh City, Vietnam

Correspondence should be addressed to Thuan Van Tran; tranuv@gmail.com and Thi Hong Nhan Le; lthnhan@hcmut.edu.vn

Received 8 March 2019; Revised 10 May 2019; Accepted 27 May 2019; Published 17 June 2019

Guest Editor: Nguuyen Van Noi

Copyright © 2019 Van Thinh Pham et al. This is an open access article distributed under the Creative Commons Attribution License, which permits unrestricted use, distribution, and reproduction in any medium, provided the original work is properly cited.

Herein, we described the use of exfoliated graphene- (EG-) decorated magnetic MnFe_2O_4 nanocomposite ($\text{EG@MnFe}_2\text{O}_4$) for the removal and adsorption of Congo red (CR) dye from wastewater. Firstly, the precursors (EG, MnFe_2O_4) and $\text{EG@MnFe}_2\text{O}_4$ were fabricated, characterized using several physical analytical techniques such as X-ray powder diffraction (XRD), scanning electron microscope (SEM), transmission electron microscopy (TEM), and N_2 adsorption/desorption isotherm measurement. For the adsorption experiments, the effect of contact time (0–240 min), concentration (10–60 mg/L), solution pH (2–10), adsorbent dosage (0.03–0.07 g), and temperature (283–313 K) was rigorously studied. To elucidate the adsorption mechanism and behaviour of CR over $\text{EG@MnFe}_2\text{O}_4$ and MnFe_2O_4 adsorbents, the kinetic models (pseudo-first-order, pseudo-second-order, Elovich, and Bangham) and isotherm models (Langmuir, Freundlich, Temkin, and Dubinin–Radushkevich) have been adopted. The kinetic results indicated that models adhered to the pseudo-second-order equation, exhibiting the chemisorption mechanism in heterogeneous phase. Meanwhile, the isotherm results revealed the adsorption of CR over $\text{EG@MnFe}_2\text{O}_4$ obeyed the monolayer behaviour (Langmuir model) rather than multilayer behaviour (Freundlich equation) over MnFe_2O_4 . The thermodynamic study also suggested that such adsorption was an endothermic and spontaneous process. With high maximum adsorption capacity (71.79 mg/g) and good recyclability (at least 4 times), $\text{EG@MnFe}_2\text{O}_4$ can be a potential alternative for the adsorptive removal of CR dye from water.

1. Introduction

Research interest in nanomaterials (metalorganic frameworks, nanoparticles, porous nanomaterials, etc.) has become an integral part in the development of future technologies [1–4]. Among these, multiferroic nanomaterials (e.g., MFe_2O_4 , M

stands for transition metals) have afforded an abundance of widely practical applications, hence, giving rise in research interests, especially in environmental remediation [5, 6]. With their outstanding properties in inherent structure, such as excellent magnetism for easy separation, high chemical stability, and tunable production in both laboratory scale and

industrial scale, many studies focused on ferrites and their modified compounds on the removal and degradation of contaminants [7–9]. Among these emergent pollutants [10–12], however, synthetic dyes (e.g., Congo red, CR) have been considered as potential carcinogenic chemicals because they can contain several toxic functional groups and nondegradable skeletons including amine, imine, and benzene rings (Scheme 1), and hence, this topic have been paid much attention over the past decades [9, 13–16].

In terms of eliminating dye compounds, some works reported the outstanding removal efficiency using ferrite nanoparticles [17–19]. For example, Wojciech et al. investigated the adsorption of acid dye Acid Red 88 using magnetic ZnFe_2O_4 spinel ferrite nanoparticles. With relatively high surface area ($139\text{ m}^2/\text{g}$), this ferroic material has given a desirable maximum adsorption capacity, at 111.1 mg/g [20]. Interestingly, Mahmoodi et al. also reported the use of sodium dodecyl sulfate (SDS) as a strongly modified agent for nickel ferrite nanoparticle (NFN) to remove a wide range of dyes including basic blue 41 (BB41), basic green 4 (BG4), and basic red 18 (BR18) with a considerable improvement in maximum adsorption capacity compared with nonmodified counterparts (control samples) [21]. These reports inspired many breakthroughs to chemically modify the ferrite structures to enhance the absorbability towards dye molecules.

Generally, the ferrites can be easily modified by coatings containing diverse functional groups, which facilitate the capture of dyes. Exfoliated graphene (EG), a typically modified material synthesizing from natural graphene, can be a brilliant candidate [22]. Although EG presents as a primary adsorbent, one of the biggest drawbacks of EG material is the difficulty to separate it from the mixture after the adsorption process due to its low density towards water [23]. Moreover, EG itself can be hardly regenerated by common methods, thus, restraining its practical applications [24]. Therefore, combination between EG and ferrites may be an optimum solution aiming at taking advantage of both attractive properties.

Herein, EG-decorated MnFe_2O_4 (namely, $\text{EG@MnFe}_2\text{O}_4$) as a promising adsorbent for the adsorption of CR as an emerging and typical dye was addressed. This material was firstly characterized using several analytical techniques such as X-ray powder diffraction (XRD), scanning electron microscope (SEM), Fourier-transform infrared spectroscopy (FT-IR), transmission electron microscopy (TEM), and N_2 adsorption/desorption isotherm measurement and used for kinetic and isotherms studies. Moreover, a series of parameters including contact time, dosage, solution pH, and temperature were employed to compare the adsorption between MnFe_2O_4 with and without EG decoration. To confirm the recyclability, $\text{EG@MnFe}_2\text{O}_4$ could be recycled for many times. To our best knowledge, its characterization and application for CR remediation was not previously addressed; hence, more investigations need to be conducted.

2. Materials and Methods

2.1. Chemicals and Instruments. Natural graphite flake (GF) was obtained from Yen Bai province, Vietnam. The material

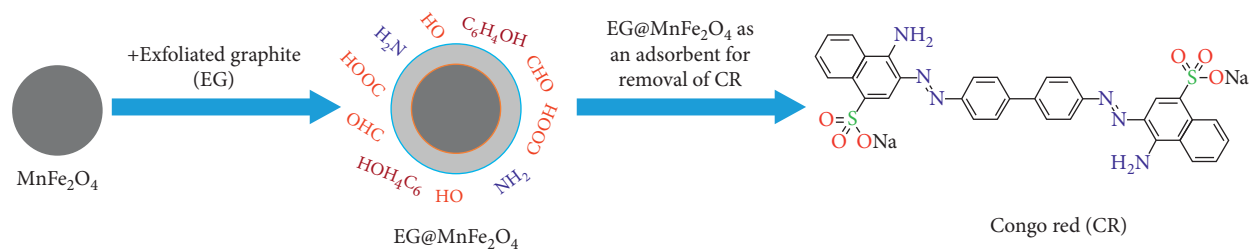
was selected to have the particle size of 60 mesh. Chemicals including Congo red, H_2SO_4 (98%), and H_2O_2 (30%) were purchased from Merck. The XRD profile was obtained using the D8 Advance Bruker powder diffractometer with $\text{Cu-K}\alpha$ beams used as excitation sources. The SEM images with the magnification of 7000x were captured with the S4800 instrument (Japan) with an accelerating voltage source (15 kV). The infrared FT-IR spectra obtained by the Nicolet 6700 spectrophotometer were used to explore the characteristics of chemical bonds and functional groups. CR concentration was determined with UV-vis spectrophotometer at wavelength of 500 nm.

2.2. Synthesis of EG. The EG porous material was produced from the natural flaky graphite source by the microwave-irradiated method [22]. Initially, flaky graphite was carefully immersed in a mixture of H_2SO_4 (98%) and H_2O_2 (30%) (100:7 by volume) at room temperature during 2 hours. Next, the chemically treated solid was repeatedly washed with H_2O and neutralized by diluted NaOH solution. The exfoliation of bulky powder was performed by the microwave-irradiated oven (750 W, 10 sec). The as-received EG sample can be collected and stored for the characterization and experiments.

2.3. Synthesis of MnFe_2O_4 . Manganese-based magnetic nanoparticle MnFe_2O_4 was produced using the conventional polymerized-complex method according to our recent work [25]. Citric acid (93 g) was mixed with 140 mL of ethylene glycol and distilled water (2:5 by volume) and heated up 80°C under air atmosphere. Then, an amount of 0.303 g- $\text{MnCl}_2\cdot 6\text{H}_2\text{O}$ solid was poured into the above mixture and heated up at 130°C . After 2 hours, the polymeric resin precursor was transferred into heat-resistant furnace and heated up at 1000°C for 2 h and allowed to cool down at room temperature. The black as-received sample can be collected and stored for the characterization and experiments.

2.4. Synthesis of $\text{EG@MnFe}_2\text{O}_4$. The synthesis procedure was followed as reported previously [26]. A mixture of 0.7 g $\text{Fe}(\text{NO}_3)_3\cdot 9\text{H}_2\text{O}$ and 0.25 g- $\text{Mn}(\text{NO}_3)_2\cdot 6\text{H}_2\text{O}$ was dissolved in 50 mL H_2O , and heated up at 90°C under stirring continuously. After that, 50 mL citric acid solution (0.02 M) was added dropwise slowly and stirred for 60 min. 0.8 g-EG was carefully poured into such solution, and then NH_3 solution was added to reach the weakly basic solution (pH 8-9). After 30 min, a slow addition of NH_3 solution for the second time into the beaker (pH 10) was employed. The mixture was dried at 80°C and calcined at 700°C during 120 min to obtain as-received sample.

2.5. Experimental Batch. To determine the absorbability of EG towards CR, batch experiments could be conducted by an addition of adsorbent (0.5 g/L) into 100 mL of dye solutions (20–60 mg/L). The samples were employed to agitate on the shaker table. Preliminary runs indicated that the adsorption process reached an equilibrium state during



SCHEME 1: Schematic process for the formation of EG@MnFe₂O₄ for the removal of Congo red.

210 min. After the adsorption completion, the adsorbent was extracted from the aqueous solution using a filter syringe, while remaining concentration of dye was measured by the UV-vis spectrophotometer at 500 nm. The removal efficiency ($H\%$) and adsorption capacity (Q) was calculated on the basis of the concentrations by the following equations:

$$H(\%) = \frac{C_0 - C_e}{C_0} \cdot 100,$$

$$Q_t = \frac{C_0 - C_t}{m} \cdot V, \quad (1)$$

$$Q_e = \frac{C_0 C_e}{m} \cdot V,$$

where C_0 and C_e are, respectively, the initial and equilibrium dye concentrations, V is the volume of solution, and m represents the weight of adsorbent.

3. Results and Discussion

3.1. Structural Characterization

3.1.1. PXRD Spectra of EG, MnFe₂O₄, and EG@MnFe₂O₄ Materials. To compare the crystallinity of EG@MnFe₂O₄ with their precursors including EG and MnFe₂O₄, the PXRD was used as a means of analysis. According to the observation from Figure 1, the profile of EG material witnessed a sharp peak at 26.6°, which was highly commensurate with previous publications, proving that EG has been successfully synthesized [27]. At a glance, the figure for MnFe₂O₄ had an apparent difference with that for EG mentioned. Indeed, there was an abundance of main peaks emerging at 24.4°, 34.0°, 36.7°, 50.0°, 54.5°, 62.5°, and 64.8°. Many works reported the same PXRD profiles of MnFe₂O₄ by various synthesis pathways (microwave-assisted ball-milling, wet-milling, solvothermal, etc.) [28–33]. The third diffraction spectrum belongs to EG@MnFe₂O₄, which had the mutual patterns of EG and MnFe₂O₄. Accordingly, a sharp peak at 26.6° again repeated at the constant position in the spectrum of EG@MnFe₂O₄ confirmed that the EG was successfully decorated in MnFe₂O₄. More interestingly, several peak traces of MnFe₂O₄ can be observed in the spectrum of EG@MnFe₂O₄. However, their signal intention seems very low, mainly because the EG may coat the peripheral shell of the MnFe₂O₄ nanoparticles. These results were totally in line with recent studies on the same structure [34–36].

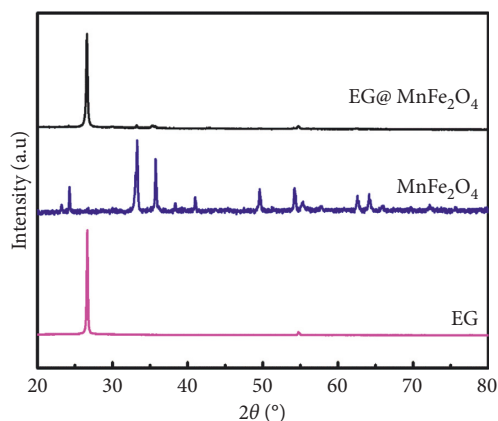


FIGURE 1: XRD spectra of EG, MnFe₂O₄, and EG@MnFe₂O₄.

3.1.2. SEM Images of EG@MnFe₂O₄ Materials. To gain more understanding about the morphological properties of EG@MnFe₂O₄ material, the SEM technique can be used. Based on the SEM images in Figure 2, which showed at two various magnification levels (50 and 100 μm), it is evident that the EG@MnFe₂O₄ structure exposed a heterogeneous, highly defective, amorphous morphology. This phenomenon may be due to the effect of a full decoration by EG nanosheets, which MnFe₂O₄ is dispersed on the flexible graphene sheet, resulting in the typical kind of rough surface of EG@MnFe₂O₄. Kalimuthu also reported the same morphology of MnFe₂O₄/graphene produced by eco-friendly hydrothermal and in situ polymerization method, offering a deep degree of wrinkled and unsmooth surface [37].

3.1.3. TEM Images of EG and EG@MnFe₂O₄ Materials. TEM technique is necessary to gain insight into inherent structure of exfoliated graphite and exfoliated graphite decorated MnFe₂O₄ materials. Figure 3 illustrates the SEM images of above materials at various scales 1 μm and 200 nm. Figures 3(a) and 3(b) show the highly opaque towards electron beams, and hence, implying that the EG obtained a thick structure [38]. In contrast, the structure of EG@MnFe₂O₄ in Figures 3(c) and 3(d) indicates a considerable difference from the EG structure. As illustrated, the existence of black spots in the opaque EG region can be due to the presence of MnFe₂O₄ particles, demonstrating the fact that MnFe₂O₄ particles were decorated by the EG sheets [39].

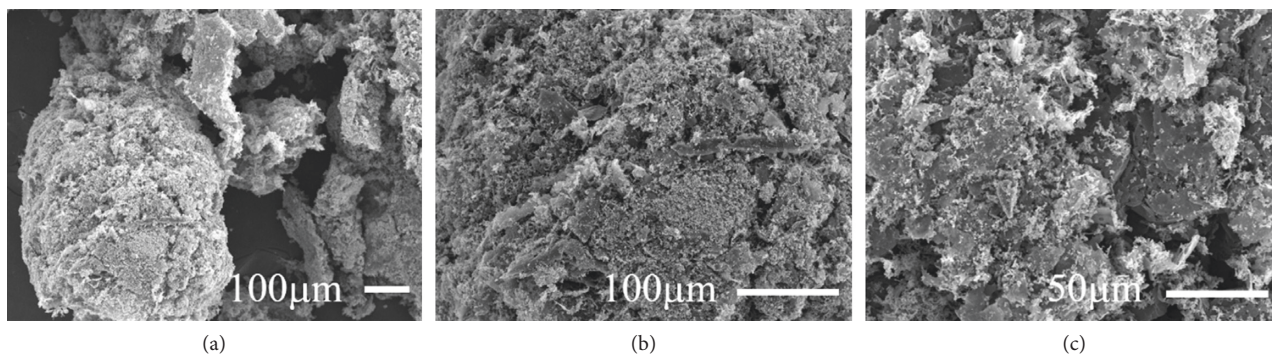


FIGURE 2: SEM images of EG@MnFe₂O₄.

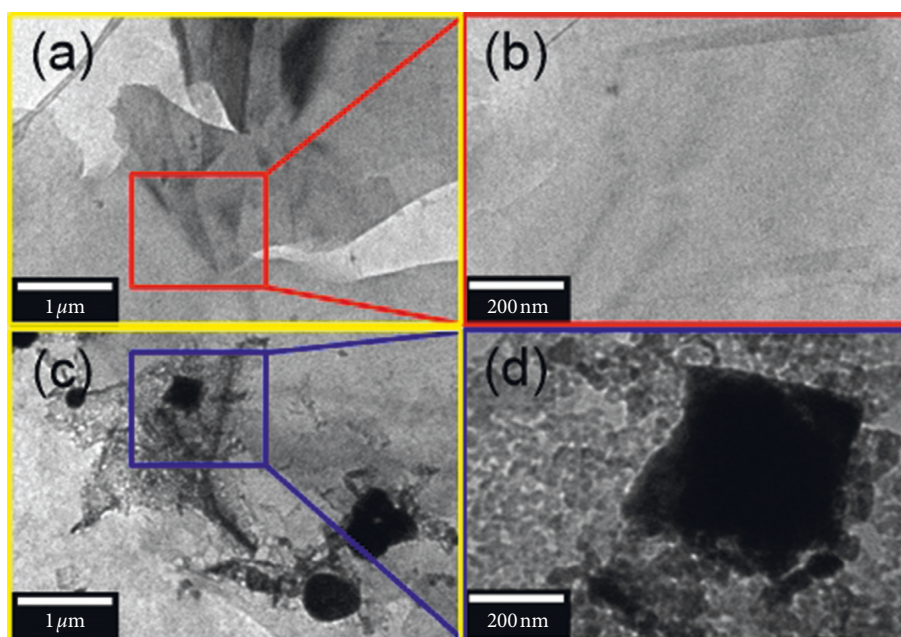


FIGURE 3: TEM images of EG (a, b) and EG@MnFe₂O₄ (c, d) materials.

3.1.4. N₂ Adsorption/Desorption Isotherm Measurement of EG and EG@MnFe₂O₄. To characterize more properties of the inherent structure, the nitrogen adsorption/desorption isotherm of EG and EG@MnFe₂O₄ can be measured at 77 K and is illustrated in Figure 4(a). Generally, these isotherms mostly exhibit no hysteresis loops, representing a type II isotherm, means that both they were likely to offer a low degree of porosity. Indeed, the surface area values calculated by BET theory and pore volume of EG and EG@MnFe₂O₄ were relatively low, but those of EG were slightly higher than those of EG@MnFe₂O₄ composite, at 33.0 m²/g, 0.1299 cm³/g compared with 40.95 m²/g, and 0.1559 cm³/g, respectively. These results can be due to the effect of aggregation under magnetism of MnFe₂O₄, resulting in the depletion in porosity in EG@MnFe₂O₄ [40, 41]. Meanwhile, pore size distribution plots of both materials in Figure 4(b) also show the existence of both micropore (<2 nm) and mesopore (2–50 nm) in their structures.

3.1.5. EDS Mapping Spectrum of EG@MnFe₂O₄. EDS mapping technique plays an important role in identifying how the components of EG@MnFe₂O₄ are included. Herein, Figure 5 shows the composition of elements existed in EG@MnFe₂O₄, which mainly consisted of carbon, iron, oxygen, and manganese. Especially, the mean content of iron in EG@MnFe₂O₄ can be measured, at 6.4%. In addition, the saturation magnetization value of EG@MnFe₂O₄ was found to be 1.5 emu/g, suggesting that EG@MnFe₂O₄ is possibly eligible to separate from an aqueous solution using a simple magnet [42, 43]. Consequently, the EG@MnFe₂O₄ structure obtained a combination of EG and MnFe₂O₄ components [34–36].

3.2. Adsorption Studies

3.2.1. Effect of pH. Theoretically, the pH is one of the most influential parameters in any adsorption process, because

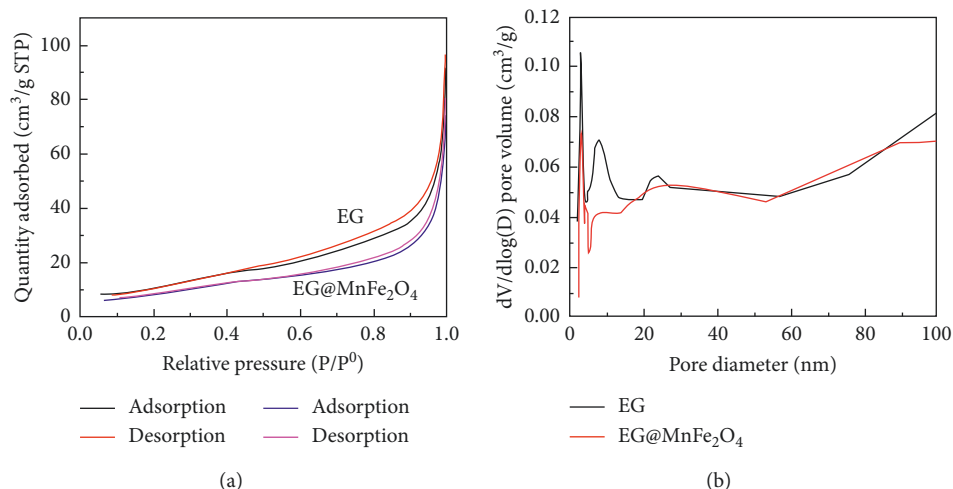


FIGURE 4: N₂ adsorption-desorption isotherm measurement (a) and pore size distribution (b) plots of EG and EG@MnFe₂O₄ materials.

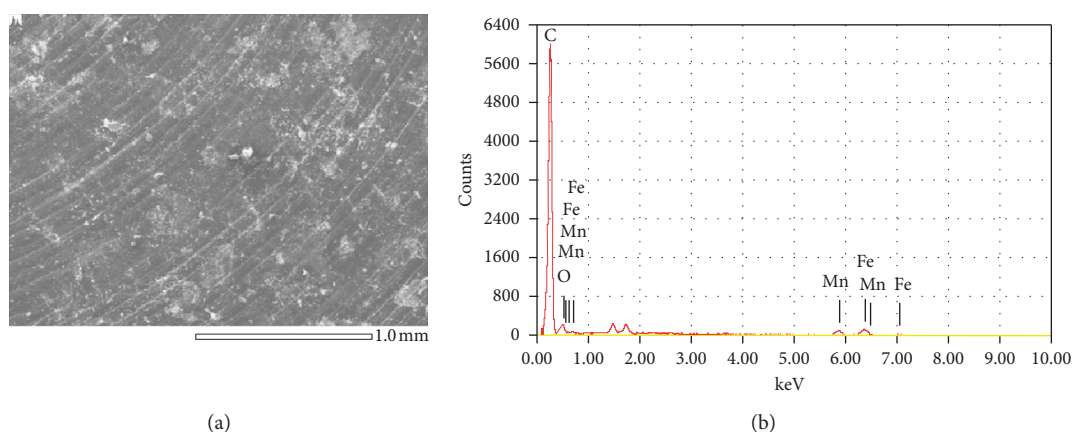


FIGURE 5: EDS mapping spectrum of EG@MnFe₂O₄.

the acidic, neutral, or basic solutions affect the charge natures (e.g., anionic, cationic, and zwitterionic) of adsorbate molecules and surface of adsorbent [44–48]. To compare the difference between MnFe₂O₄ and EG@MnFe₂O₄ materials in terms of CR adsorption efficiency, a range of pH from 2 to 12, which can be tuned by alkaline and acidic solutions, was investigated (Figure 6).

At a glance, it is evident that the adsorption uptake by EG@MnFe₂O₄ was remarkably higher than that by MnFe₂O₄ at any pH values. In detail, the highest adsorption capacity towards CR onto EG@MnFe₂O₄ could attain at nearly 66 mg/g under the pH condition of 6.0, while the optimal pH figure for MnFe₂O₄ was determined at 4.0, giving a capacity of only 35.5 mg/g. Enhancing the CR amount absorbed on EG@MnFe₂O₄ may be contributed by the component of EG coating, which contains functional groups essential for the adsorption. In our previous reports, we demonstrated the role of surface functional groups in improving the adsorption capacity of adsorbate [49, 50]. On the other hand, the CR adsorption of EG@MnFe₂O₄ by pH parameter seems to slightly drop, about 50 mg/g at the relatively weak acidic or basic media. By contrast, the adsorption of CR by

MnFe₂O₄ at neutral or strongly basic solution was highly likely to be uncondusive. These results suggested that the decoration of EG may be a considerable advantage because EG@MnFe₂O₄ material can obtain higher uptake at a harsher adsorption condition (e.g., at very strong basic/acidic solutions) in comparison to its precursor MnFe₂O₄. Based on the above results and analysis, we decided to conduct the next experiments under the pH condition at 4 and 6 for EG@MnFe₂O₄ and MnFe₂O₄ as adsorbents, respectively.

3.2.2. Effect of Dosage. Optimizing the dosage of materials is of significance to boost the cost-effectiveness in any treatment process [51]. Herein, we investigated a series of dosage by adding the amount (0.03–0.07 g) of EG@MnFe₂O₄ (a) and MnFe₂O₄ into 100 mL CR solution at the initial concentration of 60 mg/L under room temperature. After that, the concentration residuals were determined by the spectroscopy method. The effect of dosage on CR adsorption capacity was plotted and is shown in Figure 7. It is evident that the adsorption uptake by EG@MnFe₂O₄ was

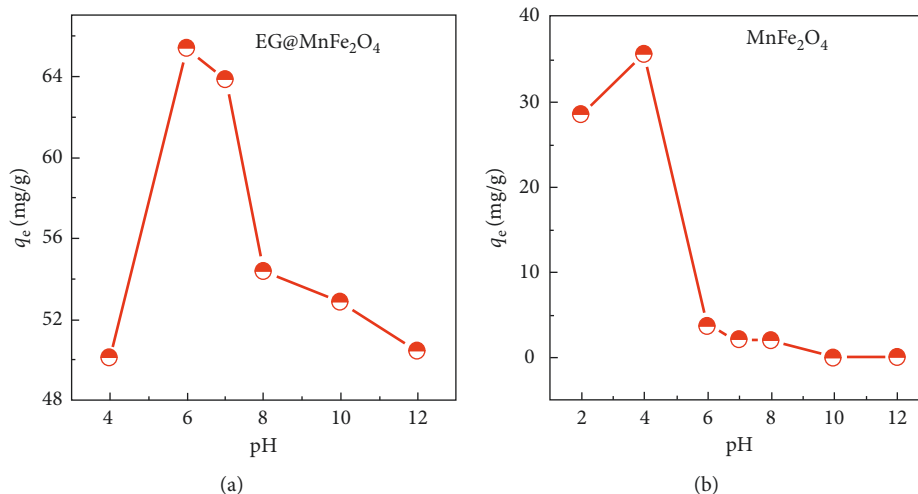


FIGURE 6: Effect of pH on the adsorption efficiency of CR over the EG@MnFe₂O₄ (a) and MnFe₂O₄ (b) materials. Experimental conditions included adsorbent dose of 0.5 g/L, solution volume of 100 mL, and dye concentration of 60 mg/L at various pH (2–12). Experiments were run at room temperature (25°C) during 210 min.

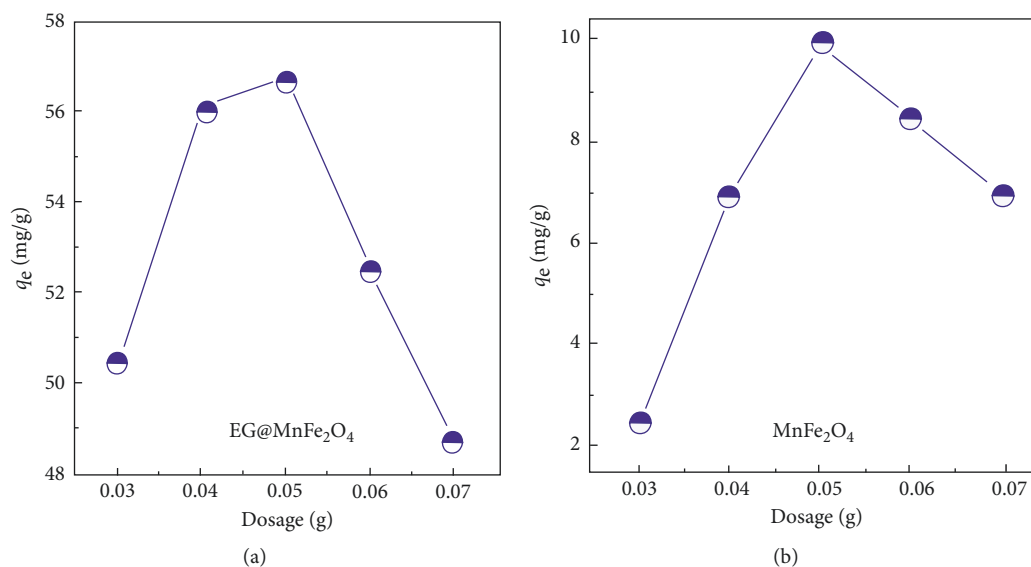


FIGURE 7: Effect of dosage the adsorption efficiency of CR over the EG@MnFe₂O₄ (a) and MnFe₂O₄ (b) materials. Experimental conditions included solution volume of 100 mL and dye concentration of 60 mg/L at pH 4 for MnFe₂O₄ and pH 6 for EG@MnFe₂O₄. Experiments were run at room temperature (25°C) during 210 min.

remarkably higher than that by MnFe₂O₄ at any dosage values. Moreover, larger amount of adsorbents (0.03–0.05 g for both EG@MnFe₂O₄ and MnFe₂O₄) led to an enhancement in CR adsorption capacity, reached the peaks of capacity at 57 and 10 mg/g, respectively. However, the adsorption efficiency rapidly dropped down until pouring higher dosage of 0.05 g. This phenomenon may be mainly due to larger amount of adsorbents resulting in hampering the mass transfer of CR molecules into the pores of materials and changing the physical properties of solution (e.g., viscosity) [52, 53]. Consequently, the optimal dosage, which compromises all factors affecting the adsorption uptake, was found at 0.05 g.

3.2.3. Effect of Contact Time and Adsorption Kinetics. According to the optimized conditions obtained from Figures 6 and 7, we carried out the kinetic experiments to investigate the influence of contact time on adsorbability towards CR of EG@MnFe₂O₄ and MnFe₂O₄ at various concentrations (20–60 mg/L). Figure 8(a) shows the plots of the adsorption capacity (Q_t , mg/g) against contact time (t , min). It is obvious that CR dye over EG@MnFe₂O₄ was rapidly absorbed during the first 60 minutes and steadily proceeded until the process became equilibrium. At the opposite trend, the plot in Figure 8(b) for MnFe₂O₄ showed a relatively gradual increase in adsorption capacity, in which adsorption at 50 mg/L gave the better adsorption results than others.

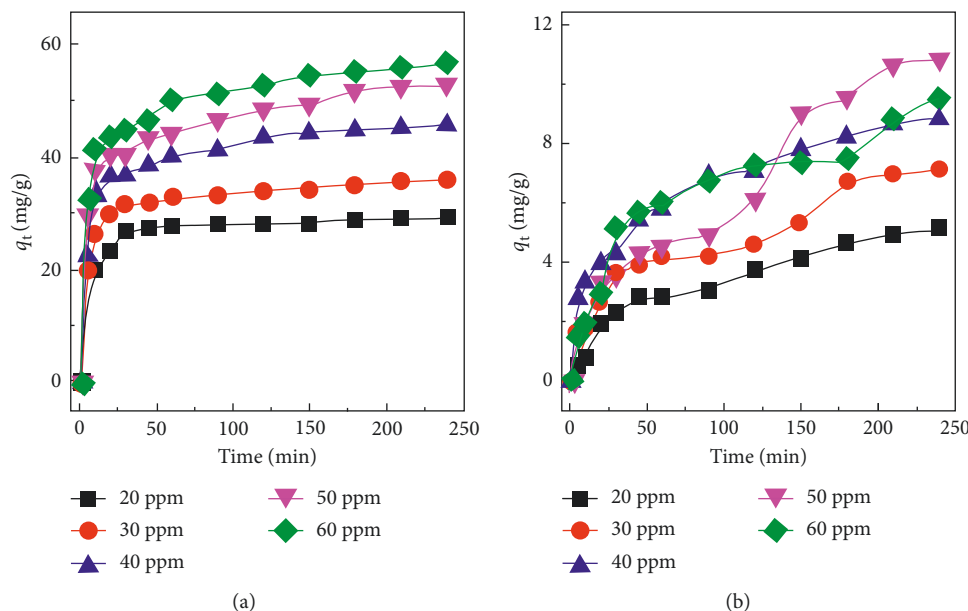


FIGURE 8: Effect of material dosage on CR adsorption capacity onto EG@MnFe₂O₄ (a) and MnFe₂O₄ (b). Experimental conditions: solution volume of 100 mL, and dye concentrations of 20–60 mg/L at pH 4 for MnFe₂O₄ and pH 6 for EG@MnFe₂O₄. Experiments were run at room temperature (25°C) during the period of 0–240 min.

To gain more insight into the profound effect of contact time, an array of commonplace kinetic equations (e.g., pseudo-first-order, pseudo-second-order, Elovich, and Bangham) were adopted and are shown in Figures 9 and 10 [52, 53]. After evaluating these models based on the coefficients of determination (R^2), adsorption mechanism in CR/EG@MnFe₂O₄ and CR/MnFe₂O₄ systems can be elucidated. Experimental data were transformed onto a mathematically linear form, which can be fitted by using the Origin Lab® version 9.0 software. Among the most prevalent kinetic models, the pseudo-first-order and pseudo-second-order models were applied herein. While equation (2) tends to explain the rate of adsorption relating to the number of unabsorbed sites from EG@MnFe₂O₄ and MnFe₂O₄, equation (3) describes the adsorption of CR over these magnetic nanocomposites through a chemisorption mechanism controlled by functional groups available on the surface of adsorbents [54].

$$\log(q_e - q_t) = \log q_e - \frac{k_1 \cdot t}{2.303}, \quad (2)$$

where k_1 (1/min) is defined as the pseudo-first-order adsorption rate constant, q_t (mg/g) is defined as the adsorption capacity at the period time t (min), and q_e (mg/g) is defined as equilibrium adsorption capacity at the equilibrium period (min).

$$\frac{t}{q_t} = \frac{1}{k_2 \cdot q_e^2} + \frac{t}{q_e}, \quad (3)$$

$$H = k_2 \cdot q_e^2, \quad (4)$$

where k_2 (g/mg min) is defined as the pseudo-second-order adsorption constant rate and H (mg/g min) is defined as initial adsorption rate (equation (4)).

Tables 1 and 2 show the parameters of these models and their respective values at five CR concentrations (20, 30, 40, 50, and 60 mg/L) by over EG@MnFe₂O₄ and MnFe₂O₄, respectively. According to Table 1, which listed kinetic parameters of the CR adsorption models over EG@MnFe₂O₄, the coefficients of determination R^2 for pseudo-second-order model (0.9987–0.9997) at all CR concentrations were far higher than those for pseudo-first-order model (0.8396–0.9749), indicating that the predicted data were well fitted with experimental data. This was also supported by Figures 9(a) and 9(b), which experimental data were depicted by the models. It is evident that the data points distributed well on the linear lines of pseudo-second-order model rather than the pseudo-first-order model. At the same trend for the CR adsorption models over MnFe₂O₄, Table 2 and Figures 10(a) and 10(b) show excellent fitness with R^2 (0.8234–0.9706) better than the others (0.6957–0.9672). Therefore, the adsorption of CR over both adsorbents obeyed the pseudo-second-order model with the dominance of chemisorption process via electrostatic attraction between adsorbent and adsorbate, while the other tends to be ineligible to explain the adsorption mechanisms. Ali et al. also reported the lower fitness of pseudo-first-order model in describing the adsorption mechanism [55]. Liu et al. proved the role of the surface functional groups in enhancing the adsorbability on modified activated carbon [56]. More interestingly, based on the values of Q_2 , the adsorption of CR over EG@MnFe₂O₄ (29.61–57.54 mg/g) was observed to be so far higher than that over MnFe₂O₄ (6.34–18.19 mg/g).

Otherwise, other two equations including (Elovich and Bangham) can be used to assess the adsorption kinetic of CR over EG@MnFe₂O₄ and MnFe₂O₄. In detail, the Elovich equation (equation (5)) assumes that the heterogeneous

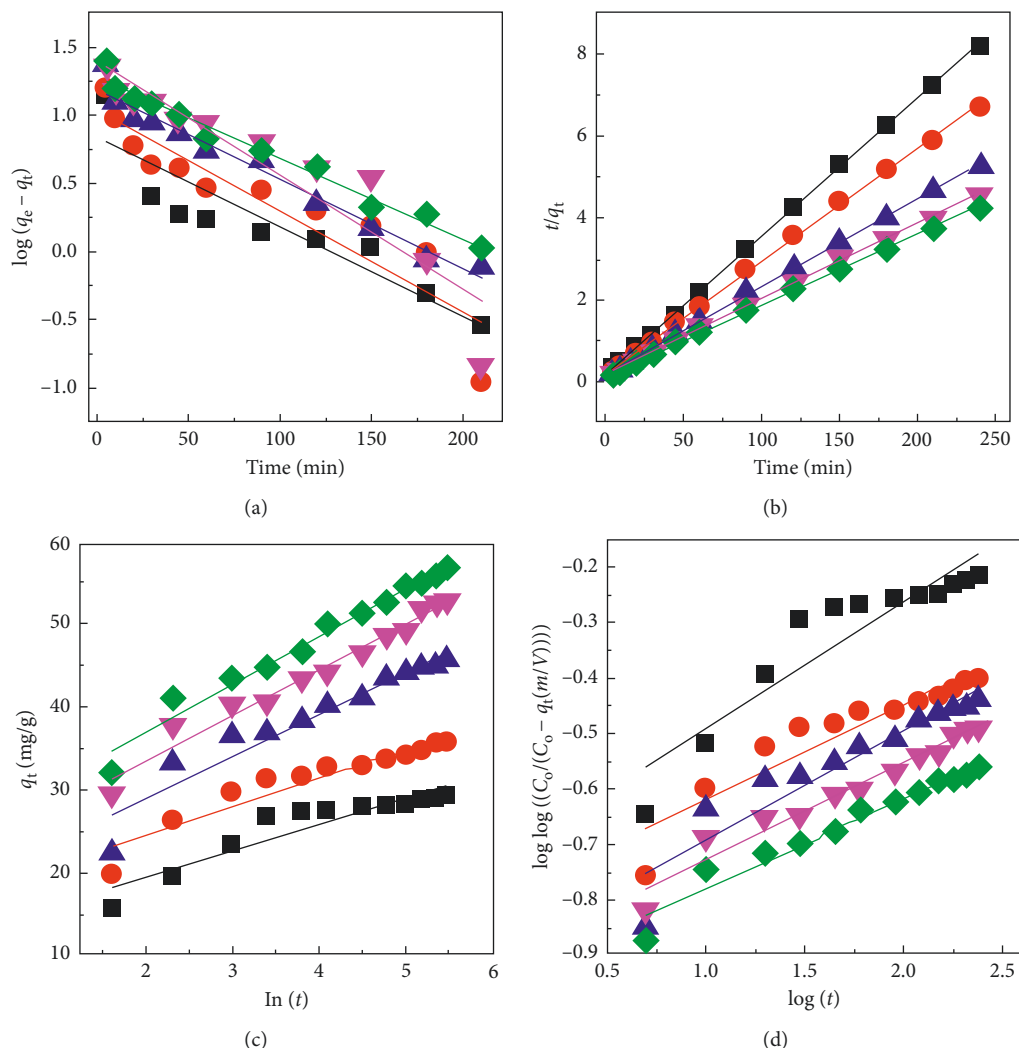


FIGURE 9: Linear plots of kinetic models: (a) pseudo-first-order, (b) pseudo-second-order, (c) Elovich, and (d) Bangham for the adsorption of CR over EG@MnFe₂O₄.

diffusion towards gases on heterogeneous surfaces or liquid/gas phase is related to the reaction rate and diffusion factor. Meanwhile, the Bangham equation (equation (6)) is typical for intraparticle diffusion mechanism of CR molecules over EG@MnFe₂O₄ and MnFe₂O₄ materials at room temperature. These equations can be described as follows:

$$Q_t = \frac{1}{\beta} \cdot \ln(\alpha \cdot \beta) + \frac{1}{\beta} \cdot \ln(t), \quad (5)$$

where α (mg/g) and β (g/mg) are defined as adsorption and desorption rates of CR molecules over EG@MnFe₂O₄ and MnFe₂O₄.

$$\log \log \left(\frac{VC_o}{VC_o - Q_t \cdot m} \right) = \log \left(\frac{k_B}{2.303 V} \right) + \alpha_B \cdot \log(t), \quad (6)$$

where k_B is defined as the Bangham equation constant and m (g) and V (mL) are defined as dosage and volume of adsorbent and solution, respectively.

According to the results from Table 1, all kinetic data by Elovich model fitted well with the experimental data due to their better goodness ($R^2 = 0.8427-0.9705$) rather than those by Bangham model ($R^2 = 0.8453-0.9512$), revealing the heterogeneous diffusion of CR over EG@MnFe₂O₄. Figures 9(c) and 9(d) were also eligible to support these results since the data points were distributed well on the linear lines of Elovich model. For analysing the adsorption data of CR onto MnFe₂O₄ via the Elovich and Bangham models, however, Figures 10(c) and 10(d) indicate the former model (0.9272–0.9901) was only better fitted with the adsorption of CR at concentrations 30–50 mg/L than the latter (0.8007–0.9616). For observation with more detail in Table 2, the CR adsorption rates (α , mg/g min) were extremely higher than CR desorption rates (β , g/mg) onto EG@MnFe₂O₄, while the figures for MnFe₂O₄ present the lower difference. This therefore follows that the adsorption of CR over EG@MnFe₂O₄ was more inclining to be favourable than over MnFe₂O₄.

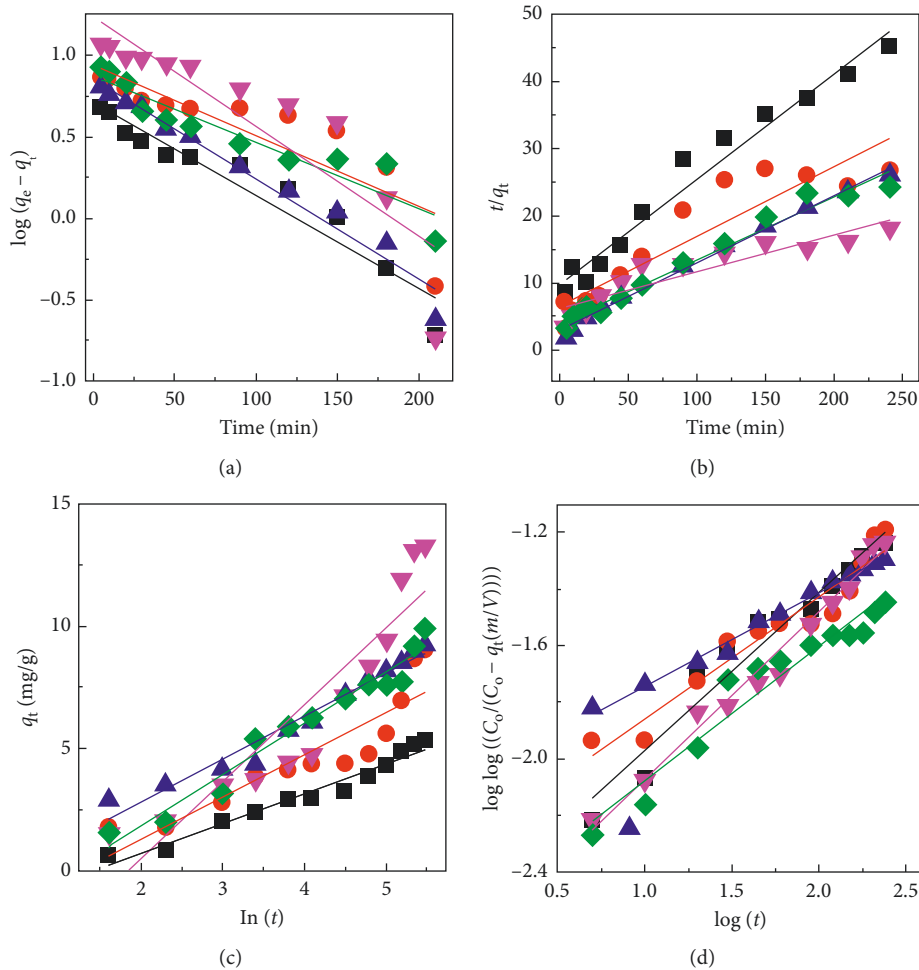


FIGURE 10: Kinetic plots of kinetic models: (a) pseudo-first-order, (b) pseudo-second-order, (c) Elovich, and (d) Bangham for the adsorption of CR over MnFe_2O_4 .

TABLE 1: Kinetic parameters of the CR adsorption models over $\text{EG@MnFe}_2\text{O}_4$.

Kinetic models	Parameters	Concentration (mg/L)				
		20	30	40	50	60
Pseudo-first-order	k_1 ($\text{min}^{-1}/(\text{mg/L})^{1/n}$)	0.0152	0.01695	0.01519	0.01920	0.01365
	Q_1 (mg/g)	6.92	10.82	15.43	24.71	18.98
	R^2	0.8396	0.8380	0.9635	0.8622	0.9749
Pseudo-second-order	$k_2 10^4$ ($\text{g}/(\text{mg}\cdot\text{min})$)	1.838	1.181	0.738	0.581	0.404
	Q_2 (mg/g)	29.61	36.10	46.51	53.82	57.54
	$H = k_2 Q_2^2$	6.2065	6.4960	6.2657	5.914	7.471
	R^2	0.9997	0.9992	0.9991	0.9974	0.9987
Elovich	β (g/mg)	0.32	0.29	0.20	0.18	0.17
	α ($\text{mg}/(\text{g}\cdot\text{min})$)	214.27	597.31	210.61	346.76	477.96
	R^2	0.8489	0.8870	0.9128	0.9683	0.9705
Bangham	k_B ($\text{mL}/(\text{g}\cdot\text{L})$)	0.0440	0.0373	0.0297	0.0289	0.0263
	α_B	0.2280	0.1717	0.1974	0.1742	0.1631
	R^2	0.8453	0.8578	0.8707	0.9571	0.9512

3.2.4. *Effect of Concentration and Adsorption Isotherms.* The isotherm models play a crucial role in better understanding the correlation between equilibrium concentration and adsorption capacity in liquid/solid phase at a constant temperature [57]. Several common isotherm

equations including Langmuir, Freundlich, Temkin, and Dubinin–Radushkevich (D–R) can be used to investigate such relationship [58–61]. To conduct adsorption isotherm investigation, the initial concentration of CR was in the range from 20 to 60 mg/L. The plots of equilibrium

TABLE 2: Kinetic parameters of the CR adsorption models over MnFe₂O₄.

Kinetic models	Parameters	Concentration (mg/L)				
		20	30	40	50	60
Pseudo-first-order	k_1 (min ⁻¹ /(mg/L) ^{1/n})	0.013	0.010	0.014	0.016	0.009
	Q_1 (mg/g)	5.12	8.67	7.13	17.31	7.42
	R^2	0.9187	0.6957	0.9672	0.7726	0.8762
Pseudo-second-order	k_2 (g/(mg·min))	0.238	0.07	0.03	0.019	0.035
	Q_2 (mg/g)	6.34	9.63	10.00	18.19	10.57
	$H = k_2 Q_2^2$	9.57	6.52	2.94	6.14	3.92
	R^2	0.9663	0.8234	0.9882	0.8312	0.9706
Elovich	β (g/mg)	0.82	0.58	0.57	0.32	0.48
	α (mg/(g·min))	2.9	4.9	1.2	0.50	0.67
	R^2	0.9592	0.8007	0.9616	0.8472	0.9558
Bangham	$k_B 10^4$ (mL/(g·L))	6.82	1.17	1.96	5.01	6.39
	α_B	0.559	0.434	0.327	0.590	0.475
	R^2	0.9439	0.9272	0.9901	0.9803	0.9333

adsorption capacity against equilibrium concentration are afforded to describe the mentioned models. In detail, the definition of four isotherms can be described as follows. Firstly, the Langmuir equation (equation (7)) assumes that the adsorption of CR molecules onto EG@MnFe₂O₄ and MnFe₂O₄ surface tends to reach the monolayer adsorption behaviour. This process may be caused by dynamically balancing the relative rates of adsorption/desorption without lateral interaction of CR molecules [62].

$$\frac{1}{Q_e} = \left(\frac{1}{Q_m K_L} \right) \frac{1}{C_e} + \frac{1}{Q_m}, \quad (7)$$

$$R_L = \frac{1}{1 + K_L C_e}, \quad (8)$$

where Q_e (mg/g), Q_m (mg/g), and C_e (mg/L) are defined as equilibrium adsorption capacity, maximum adsorption capacity, and equilibrium CR concentration, respectively. K_L (L/mg) is defined as Langmuir's constant [63]. R_L is a separate parameter and can be defined by equation (8). Based on the magnitude of R_L parameter, there are four kinds of adsorption processes: " R_L is larger than 1.0" referring to unfavourable process, " R_L is as equal as 1.0" referring to linear process, " R_L is in range from 0 to 1.0" referring to favourable process, and " R_L is as equal as 0" referring to irreversible process [64]. In addition, describing the multilayer adsorption behaviour is based on the Freundlich isotherm (equation (9)). This model proposes that the adsorption process occurs on heterogenous phase surfaces without any uniform distribution of heat of energies.

$$\ln Q_e = \ln K_F + \frac{1}{n} \ln C_e, \quad (9)$$

where K_F (mg/g) (L/mg) and $1/n$ are Freundlich's constant and exponent of nonlinearity, respectively, which can be determined from the intercept and slope of the Freundlich equation. Moreover, $1/n$ value shows the linearity of adsorption or the degree of curvature of the isotherms, and hence, its magnitude in the range from 0.1 to 0.5 indicates

the good favourability of the adsorption of CR over EG@MnFe₂O₄ and MnFe₂O₄. One of the most useful isotherm models is the Temkin equation (equation (10)), which serves to describe the influence of indirect interactions between CR molecules and "adsorption sites" of EG@MnFe₂O₄ and MnFe₂O₄ adsorbents [65].

$$Q_e = B_T \ln K_T + B_T \ln C_e, \quad (10)$$

$$B_T = \frac{RT}{b}, \quad (11)$$

where B_T , K_T (L/g), and b (J/mol) are determined from slope and intercept from equations (10) and (11). R is the ideal gas constant (8.314 J/mol·K). Finally, the Dubinin-Radushkevich (D-R) isotherm (equations (12)) is used to explain the state of chemical/physical adsorption with D-R activity coefficient B (mol²/kJ²) and adsorption capacity Q_m (mg/g), Polanyi potential ϵ (kJ/mol), and energy of adsorption E (kJ/mol), which can be calculated from equations (13) and (14):

$$\ln q_e = \ln Q_m - B\epsilon^2, \quad (12)$$

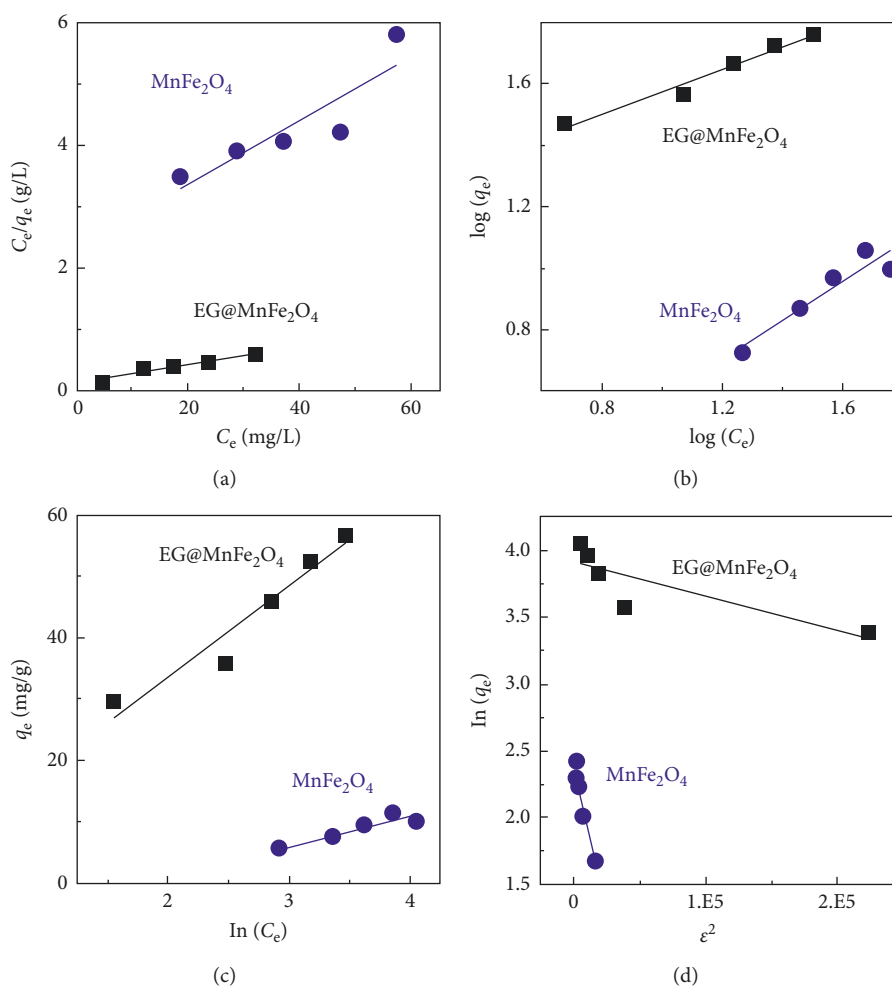
$$\epsilon = RT \ln \left(1 + \frac{1}{C_e} \right), \quad (13)$$

$$E = \frac{1}{\sqrt{-2B}}, \quad (14)$$

Table 3 lists the parameters, values, and R^2 of isotherm models for the adsorption of CR, and Figure 11 shows linear plots of isotherm models including Langmuir, Freundlich, Temkin, and D-R. It is clear that the adsorption of CR over EG@MnFe₂O₄ obeyed the Langmuir equation because of the highest R^2 (0.9572) and experimental data well fitted on the linear, assuming that the monolayer adsorption behaviour is likely to be a dominant process [66]. Meanwhile, adsorption of CR over MnFe₂O₄ adhered to the Freundlich models ($R^2 = 0.8519$), which is more inclining to occur upon multilayer adsorption behaviour. In addition, R_L (0.4–0.9) and $1/n$ (0.39–0.63) constant values confirmed that the sorption of

TABLE 3: Isotherm parameters over EG@MnFe₂O₄ and MnFe₂O₄.

Model	Parameters	Value	
		EG@MnFe ₂ O ₄	MnFe ₂ O ₄
Langmuir	k_L (L/mg)	0.0018	0.0210
	Q_m (mg/g)	71.79	19.57
	$R_L = 1/(1 + K_L C_0)$	0.90	0.44
	R^2	0.9572	0.7310
Freundlich	k_F (mg/g)/(mg/L) ^{1/n}	14.956	0.885
	1/n	0.39	0.63
	R^2	0.9274	0.8519
Temkin	k_T (L/mg)	1.00	6.01
	B_T	16.58	4.87
	R^2	0.8687	0.8205
D-R	B (kJ ² /mol ²)	2.64	0.46
	Q_m (mg/g)	50.69	11.302
	E (J/mol)	435.19	103.75
	R^2	0.5811	0.8483

FIGURE 11: Linear plots of isotherm models: (a) Langmuir, (b) Freundlich, (c) Temkin, and (d) D-R for the adsorption of CR over EG@MnFe₂O₄ and MnFe₂O₄.

CR over EG@MnFe₂O₄ and MnFe₂O₄ was the favourable process. Based on the results from Table 3, the maximum adsorption capacity (Q_m) calculated from Langmuir

equation can be found at 71.79 and 19.57 mg/g for EG@MnFe₂O₄ and MnFe₂O₄, respectively. These results are compared with those of previous studies (Table 4), showing

TABLE 4: Compared BET surface area and maximum adsorption capacity of various materials.

No.	Adsorbents	BET surface area (m ² /g)	Maximum adsorption capacity (mg/g)	Ref.
1	EG@MnFe ₂ O ₄	33.0	71.79	This study
2	MnFe ₂ O ₄	45.7	19.57	This study
3	Anilinepropylsilica xerogel	150	22.62	[67]
4	NaBentonite	25.7	35.84	[68]
5	Kaolin	20.28	5.44	[68]
6	Zeolite	8.31	3.77	[68]
7	Bentonite	32	40.4	[69]
8	Kaolin	168.8	11.88	[70]
9	Activated red mud	20.7	7.08	[71]
10	Activated coir pitch	—	6.72	[72]

the higher Q_m values than porous adsorbent mentioned. Therefore, EG@MnFe₂O₄ can be a promising candidate for the adsorption of CR in wastewater.

3.3. Thermodynamic Study. In general, the thermodynamic equation, which is represented in equation (15), can be used to diagnose the adsorption occur spontaneously or not and to elucidate the influence of temperature on the adsorption of CR over EG@MnFe₂O₄ and MnFe₂O₄. Because the determination of K_C is based on equation (16), the thermodynamic equation can be rewritten by a linear form (van't Hoff isotherm equation) as shown in equation (17).

$$\Delta G = -RT \ln K_C, \quad (15)$$

$$\ln K_C = \frac{C_A}{C_e}, \quad (16)$$

$$\ln K_C = \left(\frac{-\Delta H}{R} \right) \cdot \frac{1}{T} + \frac{\Delta S}{R}, \quad (17)$$

where K_C and T (K) are defined as the adsorption equilibrium constant and temperature, respectively; C_A (mg/g) and C_e (mg/L) are the equilibrium CR concentrations in solid phase and solution phase, respectively; ΔH (kJ/mol), ΔS (kJ/mol K), and ΔG (kJ/mol) are defined as standard enthalpy and entropy and Gibb's free energy.

Figure 12(a) plots the impact of temperature (283–313 K) on CR adsorption onto EG@MnFe₂O₄. Obviously, boosting the temperature led to a slight enhancement in the adsorption capacity. The correlation between temperature and equilibrium constant is described in Figure 11(b), which shows the plot of $\log(K_C)$ against $(1/T)$. As can be seen from Figure 12(b), experimental data were fitted well with the thermodynamic model. Moreover, high R^2 in Table 5 confirms that the van't Hoff equation obtained the excellent fitness; thus, it can be used to identify the standard thermodynamic constants (e.g., ΔH , ΔS , and ΔG). A positive ΔH reveals that the adsorption process of CR onto EG@MnFe₂O₄ tends to be endothermic. These results were highly in line with many previous works studying the adsorption of CR over various porous materials [73–77]. Meanwhile, positive value of ΔS shows an increase in disorder levels occurring in heterogeneous phase because of migration between aqueous solution and CR molecules during sorption [78]. Finally, the Gibbs free energy with minus values is

eligible to assert that the adsorption of CR on EG@MnFe₂O₄ was a spontaneous process.

3.4. Recyclability Study. On the other hand, to assess the cost-effectiveness and practical applicability of any solid adsorbent, recyclability study needs to be investigated. Herein, we selected the best materials for recyclability performance. Therefore, EG@MnFe₂O₄ can be regenerated according to the following procedure. To begin with, CR-loaded EG@MnFe₂O₄ separated from the first run was washed with 10 mL ethanol for 3 times and then with 10 mL distilled water for another 3 times. The nanomaterial was reactivated at 105°C and then used for the next use. The number of recyclability experiments was repeated to be 5 runs. The first reuse was found to be 58.41%, which was the same percentage as the standard run (60%). However, the second and third runs witnessed the slight decrease in removal efficiency, at approximately 46 and 40%. This result was commensurate with a previous work reporting about the adsorption of Congo red from aqueous solution by zeolitic imidazolate framework-8 [79]. The percentage of CR removal for another runs was rapidly dropped down. As a result, the EG@MnFe₂O₄ can be totally recycled at least four times, revealing good stability and regeneration performance of EG@MnFe₂O₄ material in eliminating the CR dye.

3.5. Proposed Mechanism. It is known that the dissociation constant (pKa) of Congo red is 4.0 [80]. In addition, we measured the point of zero charge (pH_{pzc}) of MnFe₂O₄ and EG@MnFe₂O₄ at 5.0, and 6.8, respectively. In adsorption factors, pH 6 is best condition to make the maximum removal efficiency. This can be explained based on the theory of electrostatic interaction.

In fact, at pH < pKa (CR) = 4.0, the solute tends to contain more protons, and the surface of EG@MnFe₂O₄ also becomes more positively charged. This phenomenon appears an electrostatic repulsion between the surface of EG@MnFe₂O₄ and CR cations, thus resulting in a decrease in adsorption. In contrast, when the pH value is higher than pKa of CR but lower than pH_{pzc} of EG@MnFe₂O₄, or 4.0 < pH < pH_{pzc} = 6.8, CR molecules are deprotonated to transfer a form of anion while EG@MnFe₂O₄ surface is still positively charged due to pH < pH_{pzc}. This results in an electrostatic attraction, leading to a considerable increase in

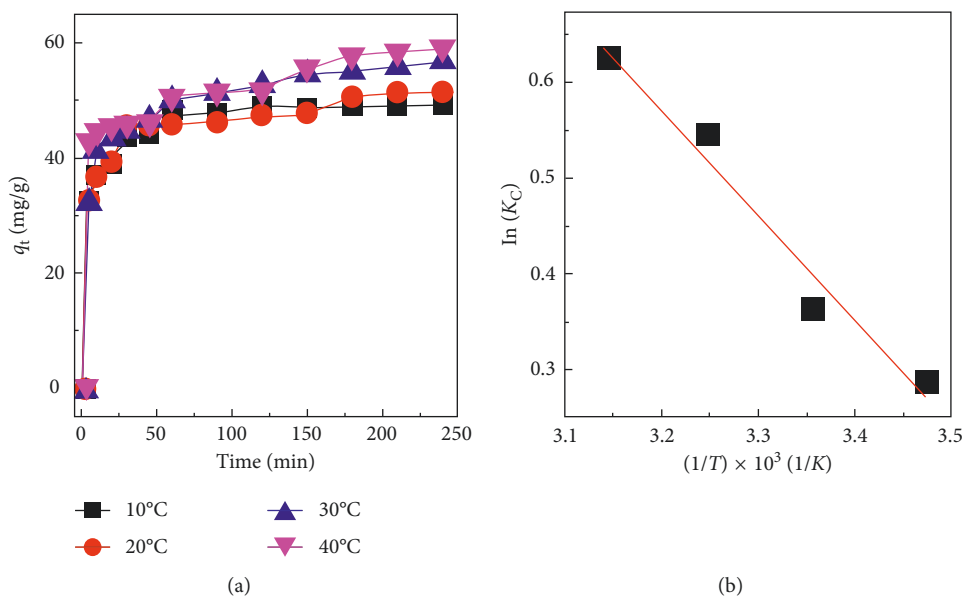


FIGURE 12: Effect of temperature on adsorption of CR over EG@MnFe₂O₄ (a) and thermodynamic study (b). Experimental conditions included solution volume of 100 mL at pH 4 for MnFe₂O₄ and pH 6 for EG@MnFe₂O₄. Experiments were run at various temperatures (10–40°C).

TABLE 5: Thermodynamic parameters for the adsorption of CR over EG@MnFe₂O₄.

van't Hoff equation	ΔH° (kJ/mol)	ΔS° (J/mol K)	ΔG_{283} (kJ/mol)	ΔG_{293} (kJ/mol)	ΔG_{303} (kJ/mol)	ΔG_{313} (kJ/mol)
$\ln K_C = -1.097(1/T) + 4.081$ $R^2 = 0.9688$	9.12	33.93	-0.652	-0.991	-1.331	-1.670

adsorption. In this study, you can see the optimum pH at 6, which is appropriate to the above analysis. However, overcoming the pH_{pzc} value tends to intercept the adsorption because both surfaces of EG@MnFe₂O₄ and CR molecules are negatively charged, causing a decline in the decontamination of CR dye. Consequently, the adsorption process is more likely to be favourable at pH varying from pK_a to pH_{pzc} .

In addition, we measured the functional groups on the surface of EG@MnFe₂O₄ with the total acidic groups (carboxylic, lactonic, and phenolic groups) at 0.096 mmol/g and total basic groups at 0.156 mmol/g, while there was no detection of any groups on MnFe₂O₄ without EG decoration. In fact, the CR adsorption capacity of EG@MnFe₂O₄ (71.79 mg/g) was found to be higher than that of MnFe₂O₄ (19.57 mg/g); therefore, these groups can have an important role in improving the adsorption. In general, the surface functional groups can create a wide range of interactions such as the H-bond, π - π interaction, n - π interaction, and electrostatic force between CR molecules and adsorbate surface [81–83]. Meanwhile, the adsorption of MnFe₂O₄ was attributable to the weak forces such as “oxygen-metal” bridge and van der Waals [54].

4. Conclusions

The present study successfully fabricated the EG, MnFe₂O₄, and EG@MnFe₂O₄ materials. The characterization results showed the EG@MnFe₂O₄ obtained a heterogeneous, highly

defective, amorphous morphology with surface area of 33 m²/g. The adsorption results showed the equilibrium time at 240 min, optimal dosage of 0.05 g and solution pH 6 for EG@MnFe₂O₄ and pH 4 for MnFe₂O₄. Moreover, kinetic and isotherm models pointed out that the adsorption of CR over EG@MnFe₂O₄ at various concentrations adhered to chemisorption mechanism (pseudo-second-order) and monolayer adsorption behaviour (Langmuir equation). In addition, the thermodynamic study confirmed that the nature of adsorption is an endothermic and spontaneous process. The maximum adsorption capacity obtained from the Langmuir model for EG@MnFe₂O₄ was calculated to be 71.79 mg/g, which was so far higher than that of MnFe₂O₄ and several previous studies, indicating that EG@MnFe₂O₄ can be a potential adsorbent for the adsorption of CR dye in water.

Data Availability

The data used to support the findings of this study are available from the corresponding author upon request.

Conflicts of Interest

The authors declare no conflicts of interest.

Acknowledgments

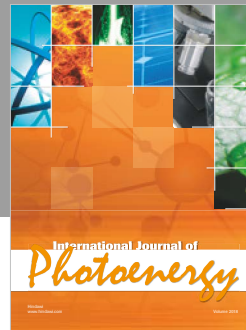
The Foundation for Science and Technology Development, Nguyen Tat Thanh University, Ho Chi Minh city, Vietnam, is acknowledged.

References

- [1] H. Q. Pham, T. T. Huynh, A. Van Nguyen, T. Van Thuan, L. G. Bach, and V. T. Thanh Ho, "Advanced Ti_{0.7}W_{0.3}O₂ nanoparticles prepared via solvothermal process using titanium tetrachloride and tungsten hexachloride as precursors," *Journal of Nanoscience and Nanotechnology*, vol. 18, no. 10, pp. 7177–7182, 2018.
- [2] T. V. Tran, H. T. N. Le, H. Q. Ha et al., "A five coordination Cu(II) cluster-based MOF and its application in the synthesis of pharmaceuticals via sp³ C-H/N-H oxidative coupling," *Catalysis Science & Technology*, vol. 7, no. 16, pp. 3453–3458, 2017.
- [3] H. T. N. Le, T. V. Tran, N. T. S. Phan, and T. Truong, "Efficient and recyclable Cu₂(BDC)₂(BPY)-catalyzed oxidative amidation of terminal alkynes: role of bipyridine ligand," *Catalysis Science & Technology*, vol. 5, no. 2, pp. 851–859, 2015.
- [4] C. Tan, X. Cao, X.-J. Wu et al., "Recent advances in ultrathin two-dimensional nanomaterials," *Chemical Reviews*, vol. 117, no. 9, pp. 6225–6331, 2017.
- [5] N. Ortega, A. Kumar, J. F. Scott, and R. S. Katiyar, "Multi-functional magnetoelectric materials for device applications," *Journal of Physics: Condensed Matter*, vol. 27, no. 50, article 504002, 2015.
- [6] M. J. Polking, A. P. Alivisatos, and R. Ramesh, "Synthesis, physics, and applications of ferroelectric nanomaterials," *MRS Communications*, vol. 5, no. 1, pp. 27–44, 2015.
- [7] A. Kanwal, H. N. Bhatti, M. Iqbal, and S. Noreen, "Basic dye adsorption onto clay/MnFe₂O₄ composite: a mechanistic study," *Water Environment Research*, vol. 89, no. 4, pp. 301–311, 2017.
- [8] X. Hou, J. Feng, Y. Ren, Z. Fan, and M. Zhang, "Synthesis and adsorption properties of sponge like porous MnFe₂O₄," *Colloids and Surfaces A: Physicochemical and Engineering Aspects*, vol. 363, no. 1–3, pp. 1–7, 2010.
- [9] W. Wang, Z. Ding, M. Cai et al., "Synthesis and high-efficiency methylene blue adsorption of magnetic PAA/MnFe₂O₄ nanocomposites," *Applied Surface Science*, vol. 346, pp. 348–353, 2015.
- [10] M. Iqbal, "Bioassays based on higher plants as excellent dosimeters for ecotoxicity monitoring: a review," *Chemistry International*, vol. 5, pp. 1–80, 2019.
- [11] M. Iqbal, "Vicia faba bioassay for environmental toxicity monitoring: a review," *Chemosphere*, vol. 144, pp. 785–802, 2016.
- [12] M. Abbas, M. Adil, S. Ehtisham-ul-Haque et al., "Vibrio fischeri bioluminescence inhibition assay for ecotoxicity assessment: a review," *Science of the Total Environment*, vol. 626, pp. 1295–1309, 2018.
- [13] S. Chatterjee, S. Chatterjee, B. P. Chatterjee, and A. K. Guha, "Adsorptive removal of Congo red, a carcinogenic textile dye by chitosan hydrobeads: binding mechanism, equilibrium and kinetics," *Colloids and Surfaces A: Physicochemical and Engineering Aspects*, vol. 299, no. 1–3, pp. 146–152, 2007.
- [14] Z. Hu, H. Chen, F. Ji, and S. Yuan, "Removal of Congo red from aqueous solution by cattail root," *Journal of Hazardous Materials*, vol. 173, no. 1–3, pp. 292–297, 2010.
- [15] N. Tahir, H. N. Bhatti, M. Iqbal, and S. Noreen, "Biopolymers composites with peanut hull waste biomass and application for crystal violet adsorption," *International Journal of Biological Macromolecules*, vol. 94, pp. 210–220, 2017.
- [16] A. Kausar, M. Iqbal, A. Javed et al., "Dyes adsorption using clay and modified clay: a review," *Journal of Molecular Liquids*, vol. 256, pp. 395–407, 2018.
- [17] X. Zhao, W. Wang, Y. Zhang, S. Wu, F. Li, and J. P. Liu, "Synthesis and characterization of gadolinium doped cobalt ferrite nanoparticles with enhanced adsorption capability for Congo red," *Chemical Engineering Journal*, vol. 250, pp. 164–174, 2014.
- [18] L. Yang, Y. Zhang, X. Liu et al., "The investigation of synergistic and competitive interaction between Congo red and methyl blue on magnetic MnFe₂O₄," *Chemical Engineering Journal*, vol. 246, pp. 88–96, 2014.
- [19] L. Wang, J. Li, Y. Wang, L. Zhao, and Q. Jiang, "Adsorption capability for Congo red on nanocrystalline MFe₂O₄ (M = Mn, Fe, Co, Ni) spinel ferrites," *Chemical Engineering Journal*, vol. 181–182, pp. 72–79, 2012.
- [20] W. Konicki, D. Sibera, E. Mijowska, Z. Lendzion-Bieluń, and U. Narkiewicz, "Equilibrium and kinetic studies on acid dye acid red 88 adsorption by magnetic ZnFe₂O₄ spinel ferrite nanoparticles," *Journal of Colloid and Interface Science*, vol. 398, pp. 152–160, 2013.
- [21] N. M. Mahmoodi, "Nickel ferrite nanoparticle: synthesis, modification by surfactant and dye removal ability," *Water, Air, & Soil Pollution*, vol. 224, no. 2, p. 1419, 2013.
- [22] T. V. Pham, T. T. Nguyen, D. T. Nguyen et al., "The preparation and characterization of expanded graphite via microwave irradiation and conventional heating for the purification of oil contaminated water," *Journal of Nanoscience and Nanotechnology*, vol. 19, no. 2, pp. 1122–1125, 2019.
- [23] Y. Si and E. T. Samulski, "Exfoliated graphene separated by platinum nanoparticles," *Chemistry of Materials*, vol. 20, no. 21, pp. 6792–6797, 2008.
- [24] M. Yi and Z. Shen, "A review on mechanical exfoliation for the scalable production of graphene," *Journal of Materials Chemistry A*, vol. 3, no. 22, pp. 11700–11715, 2015.
- [25] L. G. Bach, T. Van Tran, T. D. Nguyen, T. Van Pham, and S. T. Do, "Enhanced adsorption of methylene blue onto graphene oxide-doped XFe₂O₄ (X = Co, Mn, Ni) nanocomposites: kinetic, isothermal, thermodynamic and recyclability studies," *Research on Chemical Intermediates*, vol. 44, no. 3, pp. 1661–1687, 2018.
- [26] V. T. Pham, H.-T. T. Nguyen, D. T. C. Nguyen et al., "Process optimization by response surface methodology for adsorption of Congo red dye onto exfoliated graphite-decorated MnFe₂O₄ nanocomposite: pivotal role of surface chemistry," *Processes*, vol. 7, no. 5, p. 305, 2019.
- [27] S. Stankovich, D. A. Dikin, R. D. Piner et al., "Synthesis of graphene-based nanosheets via chemical reduction of exfoliated graphite oxide," *Carbon*, vol. 45, no. 7, pp. 1558–1565, 2007.
- [28] L. Shao, Z. Ren, G. Zhang, and L. Chen, "Facile synthesis, characterization of a MnFe₂O₄/activated carbon magnetic composite and its effectiveness in tetracycline removal," *Materials Chemistry and Physics*, vol. 135, no. 1, pp. 16–24, 2012.
- [29] Z. Zhang, Y. Wang, Q. Tan, Z. Zhong, and F. Su, "Facile solvothermal synthesis of mesoporous manganese ferrite (MnFe₂O₄) microspheres as anode materials for lithium-ion batteries," *Journal of Colloid and Interface Science*, vol. 398, pp. 185–192, 2013.
- [30] A. Han, J. Liao, M. Ye, Y. Li, and X. Peng, "Preparation of nano-MnFe₂O₄ and its catalytic performance of thermal decomposition of ammonium perchlorate," *Chinese Journal of Chemical Engineering*, vol. 19, no. 6, pp. 1047–1051, 2011.
- [31] T. Şimşek, S. Akansel, Ş. Özcan, and A. Ceylan, "Synthesis of MnFe₂O₄ nanocrystals by wet-milling under atmospheric

- conditions," *Ceramics International*, vol. 40, no. 6, pp. 7953–7956, 2014.
- [32] B. Aslibeiki, P. Kameli, M. H. Ehsani et al., "Solvothelmal synthesis of MnFe_2O_4 nanoparticles: the role of polymer coating on morphology and magnetic properties," *Journal of Magnetism and Magnetic Materials*, vol. 399, pp. 236–244, 2016.
- [33] D. Chen, Y. Zhang, and Z. Kang, "A low temperature synthesis of MnFe_2O_4 nanocrystals by microwave-assisted ball-milling," *Chemical Engineering Journal*, vol. 215–216, pp. 235–239, 2013.
- [34] Y. Yao, Y. Cai, F. Lu, F. Wei, X. Wang, and S. Wang, "Magnetic recoverable MnFe_2O_4 and MnFe_2O_4 -graphene hybrid as heterogeneous catalysts of peroxymonosulfate activation for efficient degradation of aqueous organic pollutants," *Journal of Hazardous Materials*, vol. 270, pp. 61–70, 2014.
- [35] N. Ueda Yamaguchi, R. Bergamasco, and S. Hamoudi, "Magnetic MnFe_2O_4 -graphene hybrid composite for efficient removal of glyphosate from water," *Chemical Engineering Journal*, vol. 295, pp. 391–402, 2016.
- [36] S. Li, B. Wang, B. Li, J. Liu, M. Yu, and X. Wu, "Self-assembly of 2D sandwich-structured MnFe_2O_4 /graphene composites for high-performance lithium storage," *Materials Research Bulletin*, vol. 61, pp. 369–374, 2015.
- [37] K. V. Sankar and R. K. Selvan, "The ternary MnFe_2O_4 /graphene/polyaniline hybrid composite as negative electrode for supercapacitors," *Journal of Power Sources*, vol. 275, pp. 399–407, 2015.
- [38] A. Hadi, J. Zahirifar, J. Karimi-Sabet, and A. Dastbaz, "Graphene nanosheets preparation using magnetic nanoparticle assisted liquid phase exfoliation of graphite: the coupled effect of ultrasound and wedging nanoparticles," *Ultrasonics Sonochemistry*, vol. 44, pp. 204–214, 2018.
- [39] T. V. Tran, U. T. T. Nguyen, T. T. Nguyen et al., "Synthesis and magnetic properties of graphene oxide-decorated cobalt, manganese and nickel ferrite nanoparticles prepared by polymerized route," *IOP Conference Series: Materials Science and Engineering*, vol. 479, p. 12114, 2019.
- [40] Y. Xiao, X. Li, J. Zai et al., "CoFe₂O₄-graphene nanocomposites synthesized through an ultrasonic method with enhanced performances as anode materials for Li-ion batteries," *Nano-Micro Letters*, vol. 6, no. 4, pp. 307–315, 2014.
- [41] T. Van Tran, D. T. C. Nguyen, H. T. N. Le et al., "Combined minimum-run resolution IV and central composite design for optimized removal of tetracycline drug over metal-organic framework-templated porous carbon," *Molecules*, vol. 24, no. 10, p. 1887, 2019.
- [42] H. A. Hamad, M. M. Abd El-latif, A. B. Kashyout, W. A. Sadik, and M. Y. Feteha, "Study on synthesis of superparamagnetic spinel cobalt ferrite nanoparticles as layered double hydroxides by co-precipitation method," *Russian Journal of General Chemistry*, vol. 84, no. 10, pp. 2031–2036, 2014.
- [43] M. A. E. A. Ali and H. A. Hamad, "Synthesis and characterization of highly stable superparamagnetic CoFe_2O_4 nanoparticles as a catalyst for novel synthesis of thiazolo [4, 5-b] quinolin-9-one derivatives in aqueous medium," *Journal of Molecular Catalysis A: Chemical*, vol. 404–405, pp. 148–155, 2015.
- [44] T. V. Tran, D. T. C. Nguyen, H. T. N. Le et al., "Tunable synthesis of mesoporous carbons from $\text{Fe}_3\text{O}(\text{BDC})_3$ for chloramphenicol antibiotic remediation," *Nanomaterials*, vol. 9, no. 2, p. 237, 2019.
- [45] M. Elkady, H. Shokry, and H. Hamad, "Microwave-assisted synthesis of magnetic hydroxyapatite for removal of heavy metals from groundwater," *Chemical Engineering & Technology*, vol. 41, no. 3, pp. 553–562, 2018.
- [46] N. A. El Essawy, S. M. Ali, H. A. Farag, A. H. Konsowa, M. Elnouby, and H. A. Hamad, "Green synthesis of graphene from recycled PET bottle wastes for use in the adsorption of dyes in aqueous solution," *Ecotoxicology and Environmental Safety*, vol. 145, pp. 57–68, 2017.
- [47] S. E. A. Elhafez, H. A. Hamad, A. A. Zaatout, and G. F. Malash, "Management of agricultural waste for removal of heavy metals from aqueous solution: adsorption behaviors, adsorption mechanisms, environmental protection, and techno-economic analysis," *Environmental Science and Pollution Research*, vol. 24, no. 2, pp. 1397–1415, 2017.
- [48] M. El kady, H. Shokry, and H. Hamad, "Effect of superparamagnetic nanoparticles on the physicochemical properties of nano hydroxyapatite for groundwater treatment: adsorption mechanism of Fe(ii) and Mn(ii)," *RSC Advances*, vol. 6, no. 85, pp. 82244–82259, 2016.
- [49] T. Van Tran, D. T. Cam Nguyen, H. T. N. Le et al., "A hollow mesoporous carbon from metal-organic framework for robust adsorbability of ibuprofen drug in water," *Royal Society Open Science*, vol. 6, no. 5, article 190058, 2019.
- [50] T. Van Tran, D. T. C. Nguyen, H. T. N. Le et al., "Facile synthesis of manganese oxide-embedded mesoporous carbons and their adsorbability towards methylene blue," *Chemosphere*, vol. 227, pp. 455–461, 2019.
- [51] T. V. Tran, D. T. C. Nguyen, H. T. N. Le et al., "MIL-53 (Fe)-directed synthesis of hierarchically mesoporous carbon and its utilization for ciprofloxacin antibiotic remediation," *Journal of Environmental Chemical Engineering*, vol. 7, no. 1, article 102881, 2019.
- [52] M. R. Esfahani, E. M. Languri, and M. R. Nunna, "Effect of particle size and viscosity on thermal conductivity enhancement of graphene oxide nanofluid," *International Communications in Heat and Mass Transfer*, vol. 76, pp. 308–315, 2016.
- [53] K. Wang, L. Zhang, W. Zhang, and G. Luo, "Mass-transfer-controlled dynamic interfacial tension in microfluidic emulsification processes," *Langmuir*, vol. 32, no. 13, pp. 3174–3185, 2016.
- [54] T. V. Tran, V. D. Cao, V. H. Nguyen et al., "MIL-53 (Fe) derived magnetic porous carbon as a robust adsorbent for the removal of phenolic compounds under the optimized conditions," *Journal of Environmental Chemical Engineering*, article 102902, 2019.
- [55] R. M. Ali, H. A. Hamad, M. M. Hussein, and G. F. Malash, "Potential of using green adsorbent of heavy metal removal from aqueous solutions: adsorption kinetics, isotherm, thermodynamic, mechanism and economic analysis," *Ecological Engineering*, vol. 91, pp. 317–332, 2016.
- [56] Y. Liu, X. Liu, W. Dong, L. Zhang, Q. Kong, and W. Wang, "Efficient adsorption of sulfamethazine onto modified activated carbon: a plausible adsorption mechanism," *Scientific Reports*, vol. 7, no. 1, article 12437, 2017.
- [57] T. Van Tran, Q. T. P. Bui, T. D. Nguyen, V. T. T. Ho, and L. G. Bach, "Application of response surface methodology to optimize the fabrication of ZnCl_2 -activated carbon from sugarcane bagasse for the removal of Cu^{2+} ," *Water Science and Technology*, vol. 75, no. 9, pp. 2047–2055, 2017.
- [58] D. Balarak, F. Mostafapour, H. Azarpira, and A. Joghataei, "Mechanisms and equilibrium studies of sorption of

- metronidazole using graphene oxide," *Journal of Pharmaceutical Research International*, vol. 19, no. 4, pp. 1–9, 2017.
- [59] D.A.O, A. P. Olalekan, A. M. Olatunya, and O. Dada, "Langmuir, Freundlich, Temkin and dubinin-radushkevich isotherms studies of equilibrium sorption of Zn^{2+} unto phosphoric acid modified rice husk," *IOSR Journal of Applied Chemistry*, vol. 3, no. 1, pp. 38–45, 2012.
- [60] C. Nguyen and D. D. Do, "The Dubinin-Radushkevich equation and the underlying microscopic adsorption description," *Carbon*, vol. 39, no. 9, pp. 1327–1336, 2001.
- [61] S. Azizian, M. Haerifar, and J. Basiri-Parsa, "Extended geometric method: a simple approach to derive adsorption rate constants of Langmuir-Freundlich kinetics," *Chemosphere*, vol. 68, no. 11, pp. 2040–2046, 2007.
- [62] V. T. Tran, D. T. Nguyen, V. T. T. Ho, P. Q. H. Hoang, P. Q. Bui, and L. G. Bach, "Efficient removal of Ni^{2+} ions from aqueous solution using activated carbons fabricated from rice straw and tea waste," *Journal of Material and Environmental Sciences*, vol. 8, pp. 426–437, 2017.
- [63] P. S. Ghosal and A. K. Gupta, "Determination of thermodynamic parameters from Langmuir isotherm constant-revisited," *Journal of Molecular Liquids*, vol. 225, pp. 137–146, 2017.
- [64] T. Van Tran, Q. T. P. Bui, T. D. Nguyen, N. T. H. Le, and L. G. Bach, "A comparative study on the removal efficiency of metal ions (Cu^{2+} , Ni^{2+} , and Pb^{2+}) using sugarcane bagasse-derived $ZnCl_2$ -activated carbon by the response surface methodology," *Adsorption Science & Technology*, vol. 35, no. 1-2, pp. 72–85, 2017.
- [65] D. T. C. Nguyen, "Metal-organic framework MIL-53(Fe) as an adsorbent for ibuprofen drug removal from aqueous solutions: response surface modeling and optimization," *Journal of Chemistry*, vol. 2019, Article ID 5602957, 11 pages, 2019.
- [66] T. Van Thuan, B. T. P. Quynh, T. D. Nguyen, V. T. T. Ho, and L. G. Bach, "Response surface methodology approach for optimization of Cu^{2+} , Ni^{2+} and Pb^{2+} adsorption using KOH-activated carbon from banana peel," *Surfaces and Interfaces*, vol. 6, pp. 209–217, 2017.
- [67] F. A. Pavan, S. L. P. Dias, E. C. Lima, and E. V. Benvenutti, "Removal of congo red from aqueous solution by aniline-propylsilica xerogel," *Dyes and Pigments*, vol. 76, no. 1, pp. 64–69, 2008.
- [68] V. Vimonses, S. Lei, B. Jin, C. W. K. Chow, and C. Saint, "Kinetic study and equilibrium isotherm analysis of congo red adsorption by clay materials," *Chemical Engineering Journal*, vol. 148, no. 2-3, pp. 354–364, 2009.
- [69] M. A. Akl, A. M. Youssef, and M. M. Al-Awadhi, "Adsorption of acid dyes onto bentonite and surfactant-modified bentonite," *Journal of Analytical & Bioanalytical Techniques*, vol. 4, no. 4, pp. 3–7, 2013.
- [70] I. D. Mall, V. C. Srivastava, N. K. Agarwal, and I. M. Mishra, "Removal of congo red from aqueous solution by bagasse fly ash and activated carbon: kinetic study and equilibrium isotherm analyses," *Chemosphere*, vol. 61, no. 4, pp. 492–501, 2005.
- [71] A. Tor and Y. Cengeloglu, "Removal of congo red from aqueous solution by adsorption onto acid activated red mud," *Journal of Hazardous Materials*, vol. 138, no. 2, pp. 409–415, 2006.
- [72] C. Namasivayam and D. Kavitha, "Removal of congo red from water by adsorption onto activated carbon prepared from coir pith, an agricultural solid waste," *Dyes and Pigments*, vol. 54, no. 1, pp. 47–58, 2002.
- [73] T. Şişmanoğlu and G. S. Pozan, "Adsorption of congo red from aqueous solution using various TiO_2 nanoparticles," *Desalination and Water Treatment*, vol. 57, no. 28, pp. 13318–13333, 2016.
- [74] M. Foroughi-Dahr, H. Abolghasemi, M. Esmaili, A. Shojamoradi, and H. Fatoorehchi, "Adsorption characteristics of Congo red from aqueous solution onto tea waste," *Chemical Engineering Communications*, vol. 202, no. 2, pp. 181–193, 2015.
- [75] K. S. P.-M. Adolphe, T. G. Merlain, L. N. R. Blaise et al., "Kinetics and equilibrium studies of the adsorption of nickel (II) ions from aqueous solution onto modified natural and synthetic iron oxide," *International Journal of Basic and Applied Sciences*, vol. 4, no. 3, p. 277, 2015.
- [76] T. M. Rao and V. V. B. Rao, "Biosorption of congo red from aqueous solution by crab shell residue: a comprehensive study," *Springerplus*, vol. 5, no. 1, p. 537, 2016.
- [77] Y. Zhou, L. Ge, N. Fan, and M. Xia, "Adsorption of congo red from aqueous solution onto shrimp shell powder," *Adsorption Science & Technology*, vol. 36, no. 5-6, pp. 1310–1330, 2018.
- [78] H. Guedidi, L. Reinert, J.-M. Lévêque, Y. Soneda, N. Bellakhal, and L. Duclaux, "The effects of the surface oxidation of activated carbon, the solution pH and the temperature on adsorption of ibuprofen," *Carbon*, vol. 54, pp. 432–443, 2013.
- [79] C. Jiang, B. Fu, H. Cai, and T. Cai, "Efficient adsorptive removal of congo red from aqueous solution by synthesized zeolitic imidazolate framework-8," *Chemical Speciation & Bioavailability*, vol. 28, no. 1–4, pp. 199–208, 2016.
- [80] C. Wu, J. Scott, and J.-E. Shea, "Binding of congo red to amyloid protofibrils of the alzheimer β 9-40 peptide probed by molecular dynamics simulations," *Biophysical Journal*, vol. 103, no. 3, pp. 550–557, 2012.
- [81] H. N. Tran, Y.-F. Wang, S.-J. You, and H.-P. Chao, "Insights into the mechanism of cationic dye adsorption on activated charcoal: the importance of π - π interactions," *Process Safety and Environmental Protection*, vol. 107, pp. 168–180, 2017.
- [82] H. N. Tran, H.-P. Chao, and S.-J. You, "Activated carbons from golden shower upon different chemical activation methods: synthesis and characterizations," *Adsorption Science & Technology*, vol. 36, no. 1-2, pp. 95–113, 2017.
- [83] H. N. Tran, S.-J. You, and H.-P. Chao, "Insight into adsorption mechanism of cationic dye onto agricultural residues-derived hydrochars: negligible role of π - π interaction," *Korean Journal of Chemical Engineering*, vol. 34, no. 6, pp. 1708–1720, 2017.



Hindawi

Submit your manuscripts at
www.hindawi.com

